MATHEMATICAL ENGINEERING
TECHNICAL REPORTS

A Non-Interior Implicit Smoothing Approach to Complementarity Problems for Frictionless Contacts

Yoshihiro KANNO and Makoto OHSAKI

METR 2009–06 March 2009

DEPARTMENT OF MATHEMATICAL INFORMATICS
GRADUATE SCHOOL OF INFORMATION SCIENCE AND TECHNOLOGY
THE UNIVERSITY OF TOKYO
BUNKYO-KU, TOKYO 113-8656, JAPAN

WWW page: http://www.keisu.t.u-tokyo.ac.jp/research/techrep/index.html

A Non-Interior Implicit Smoothing Approach to Complementarity Problems for Frictionless Contacts

Yoshihiro Kanno [a,†] , Makoto Ohsaki [b,‡]

[a] *Department of Mathematical Informatics, University of Tokyo, Tokyo 113-8656, Japan*

[b] *Department of Architecture and Architectural Engineering, Kyoto University, Kyoto 615-8540, Japan*

Abstract

This paper presents a non-interior point method for a frictionless contact problem in the large deformation, where we can exploit the warm start condition in an incremental path-following method such as the arc-length method. We propose a novel reformulation of the nonlinear complementarity problem based on the smoothed Fischer–Burmeister function, in which the smoothing parameter is considered as an independent variable, and we add a nonlinear equation so that the smoothing parameter behaves as a measure of the residual of the complementarity conditions. The reduced system of nonlinear equations is solved by using a conventional method for nonlinear equations with a fast local convergence from the initial point which is defined by using the solution of the previous loading stage. Throughout numerical examples it is shown that in many cases the solution can be found within four iterations.

Keywords

Contact problem; Complementarity problem; Smoothing method; Fischer–Burmeister function; Arc-length method.

1 Introduction

Contact problems in large deformations are of particular importance in wide range of engineering application [20, 38]. In this paper we investigate a new formulation for an equilibrium path-following method of unilateral frictionless contacts from the view point of a sequence of perturbed complementarity problems where the solution to an old problem can be used as a good initial point for a new one.

Various numerical methods have been presented for contact problems. A continuation method was presented by Miersemann and Mittelmann [23] which traces an equilibrium path with limit

[†]Corresponding author. Address: Department of Mathematical Informatics, Graduate School of Information Science and Technology, University of Tokyo, Tokyo 113-8656, Japan. E-mail: kanno@mist.i.u-tokyo.ac.jp. Phone: +81-3-5841-6906, Fax: +81-3-5841-6886.

[‡]Address: Department of Architecture and Architectural Engineering, Graduate School of Engineering, Kyoto University, Nishikyo, Kyoto 615-8540, Japan. E-mail: ohsaki@archi.kyoto-u.ac.jp. Phone: +81-75-383-2901, Fax: +81-75-383-2972.

points in frictionless contact problems. Zavarise *et al.* [40] solved contact problems by a combination of penalty and barrier methods. Augmented Lagrangian methods have been studied extensively for large deformation contact problems [20, 27].

It is known that frictionless/frictional contact problems can be formulated as complementarity problems. Hence, solution methods for complementarity problems may be applicable to contact problems. Roughly speaking, numerical algorithms for complementarity problems fall into three categories. The first class is known as the nonsmooth method [7, 8, 25, 26, 30], in which a complementarity problem is reformulated as a system of nondifferentiable equations and solved by using a nonsmooth Newton method. Pang [25] proposed a B-differentiable Newton method, which was applied to frictional/frictionless contact problem [1, 5]. Christensen [4] solved elasto-plastic frictional contact problems by using a semismooth Newton method [6]. The second class is the so-called smoothing method [2, 16, 22, 29, 31, 43], in which we solve a sequence of differentiable approximations to the original nondifferentiable problem. Algorithms based on smoothing methods were proposed for frictional contacts [14, 21, 41, 42]. The third one is the interior-point method [17, 28, 35–37, 44], in which a sequence of perturbed complementarity problems is solved. The step size is determined so that the inequality constraints are satisfied at each iteration. Christensen *et al.* [5] applied the interior-point method for constrained equation [37] to frictional contacts. The authors performed frictionless contact analysis of cable networks by using the interior-point method for second-order cone programs [15].

This paper discusses a smoothing method for frictionless contacts in large deformations. Particularly we focus on a warm start condition, when we solve a sequence of perturbed complementarity problems. Such a situation arises in the procedure of the incremental path-tracing analysis of frictionless contacts: it is natural to expect that the solution at the equilibrium state corresponding to the previous loading stage can be utilized as a good initial point for the complementarity problem corresponding to the current loading stage. This motivates us to propose a new reformulation of the complementarity problem which is suitable for a warm start condition.

Consider a complementarity problem

$$\boldsymbol{y} = \boldsymbol{f}(\boldsymbol{x}), \tag{1}$$

$$x_i \geq 0, \quad y_i \geq 0, \quad x_i y_i = 0, \qquad i = 1, \ldots, N, \tag{2}$$

where $\boldsymbol{f} : \mathbb{R}^N \to \mathbb{R}^N$ is continuously differentiable. For solving the complementarity problem the major difficulty is to deal with the complementarity conditions, (2). We call $\psi : \mathbb{R}^2 \to \mathbb{R}$ a complementarity function if $\psi(a, b) = 0$ holds if and only if $a \geq 0$, $b \geq 0$, and $ab = 0$ [9]. There are many choices for the function ψ. It is immediate that (2) is reduced to

$$\psi(x_i, y_i) = 0, \qquad i = 1, \ldots, N. \tag{3}$$

In nonsmooth methods, with a choice of nonsmooth ψ, the system of (1) and (3) is solved by using a nonsmooth Newton method. In contrast, in smoothing methods (2) is replaced with

$$\hat{\psi}(x_i, y_i; \varepsilon) = 0, \qquad i = 1, \ldots, N, \tag{4}$$

where $\varepsilon > 0$ is a constant, $\hat{\psi}(\,\cdot\,; 0) : \mathbb{R}^2 \to \mathbb{R}$ is a complementarity function, and $\hat{\psi}(\,\cdot\,; \varepsilon)$ is continuously differentiable for any $\varepsilon > 0$. Then the system of differentiable nonlinear equations, (1) and

(4), is solved sequentially by gradually decreasing ε to zero from a sufficiently large initial value. In most of interior-points we perturb (2) as

$$x_i y_i = \varepsilon, \qquad i = 1, \ldots, N, \tag{5}$$

$$x_i > 0, \quad y_i > 0, \qquad i = 1, \ldots, N. \tag{6}$$

By gradually decreasing ε from a sufficiently large initial value, we solve a sequence of differentiable equations, (1) and (5), to obtain the search directions, where the line search is performed so that (6) is satisfied at each iteration.

In the incremental path-tracing method, as mentioned above, the solution at the previous loading stage may be expected to be close to the solution at the current stage, but is not an interior solution in general. In such a case, an interior-point method should be started from a quite large value of ε in order to recover (6). Even if (6) is satisfied at an initial point, it is close to the boundary of the feasible set, because the complementarity conditions, (2), are satisfied at the previous equilibrium state. In such a case the step size of an interior-point method has to be very small in order to retain (6). Thus, it is not easy to exploit a warm start condition of this point with the interior-point method, which motivates us to investigate a non-interior point method.

Among non-interior point methods we focus on a smoothing method so that we can utilize standard commercial software for differentiable nonlinear equations. However, in (4), there exists only a heuristic way to choose an initial value for ε compatible to the given initial values of $\boldsymbol{x}$ and $\boldsymbol{y}$. Moreover, it is desired to decrease the amount of ε adequately, because too rapid reduction of ε is not suitable for avoiding the nonsmooth property of $\hat{\psi}(\cdot; 0)$, and too slow reduction causes unnecessary iterations. To deal with these issues we propose to reformulate (2) as

$$\hat{\psi}(x_i, y_i; \varepsilon) = 0, \qquad i = 1, \ldots, N, \tag{7}$$

$$\eta_1(\boldsymbol{x}^{\mathrm{T}}\boldsymbol{y}/N) = \eta_2(\varepsilon) \tag{8}$$

with differentiable η_1, $\eta_2 : \mathbb{R} \to \mathbb{R}$ satisfying some conditions, where ε is considered as an independent variable; see section 3 for details. This idea corresponds to a natural extension of implicit reformulation approaches proposed for the mathematical program with equilibrium constraints in the complementarity form [11–13]. Then we solve $(2N+1)$ nonlinear equations, (1), (7), and (8), in the $(2N+1)$ variables by using a conventional method for differentiable equations with a fast local convergence, e.g. the Newton method, the trust-region method, etc. We impose some conditions on η_1 and η_2 so that (8) makes ε proportional to the residual of complementarity conditions, $\boldsymbol{x}^{\mathrm{T}}\boldsymbol{y}$. This is our key idea to exploit a warm start condition for a perturbed complementarity problem. Hence, an adequate initial value for ε can be assigned by using (8). Moreover, $|\varepsilon|$ is decreased automatically as $|\boldsymbol{x}^{\mathrm{T}}\boldsymbol{y}|$ decreases in a usual procedure of a solution method for nonlinear equations.

This paper is organized as follows. As preliminaries, section 2 formulates the frictionless contact problem in large deformation as a complementarity problem. In section 3 we present an essential idea for reformulating a complementarity problem into an implicit formulation with an auxiliary variable. Section 4 describes details of our non-interior point approach to the arc-length method, in which we exploit a warm start condition. Numerical results are shown in section 5; convergence properties from an initial point far from the solution is investigated in section 5.1, and the efficiency

of the warm start strategy is examined in sections 5.2 and 5.3. Finally, conclusions are drawn in section 6.

A few words regarding our notation: all vectors are assumed to be column vectors. The $(m+n)$-dimensional column vector $(\boldsymbol{u}^{\mathrm{T}}, \boldsymbol{v}^{\mathrm{T}})^{\mathrm{T}}$ consisting of $\boldsymbol{u} \in \mathbb{R}^m$ and $\boldsymbol{v} \in \mathbb{R}^n$ is often written simply as $(\boldsymbol{u}, \boldsymbol{v})$. We write $\boldsymbol{p} \geq \boldsymbol{0}$ for $\boldsymbol{p} = (p_i) \in \mathbb{R}^n$ if $p_i \geq 0$ $(i = 1, \ldots, n)$. For $\boldsymbol{q} : \mathbb{R}^n \to \mathbb{R}$ we denote by $\nabla \boldsymbol{g}(\boldsymbol{x})$ its gradient at $\boldsymbol{x}$, i.e. $\nabla \boldsymbol{g}(\boldsymbol{x}) = (\partial g_i / \partial x_j \mid i, j = 1, \ldots, n)$. We denote by $\boldsymbol{1}$ the vector $(1, \ldots, 1)^{\mathrm{T}} \in \mathbb{R}^n$ without specifying n, unless it is not clear from the context.

2 Formulation as nonlinear complementarity problem

Consider an elastic body which is loaded and may possibly make frictionless unilateral contact with some fixed rigid obstacles. The body is discretized to finite elements so that its deformed state is represented by the displacement vector $\boldsymbol{u} \in \mathbb{R}^d$, where d is the number of degrees of freedom of displacements.

Let $\pi : \mathbb{R}^d \to \mathbb{R}$ denote the strain energy function, which is assumed to be twice continuously differentiable. The internal forces are given by $-\nabla \pi(\boldsymbol{u})$. We denote by $\lambda \boldsymbol{f}$ the external load, where $\boldsymbol{f} \in \mathbb{R}^d$ is a specified vector of the force pattern, and $\lambda \in \mathbb{R}$ is a loading parameter. Consequently, the total potential energy is written as $\pi(\boldsymbol{u}) - \lambda \boldsymbol{f}^{\mathrm{T}} \boldsymbol{u}$.

Let $\mathcal{P}_{\mathrm{c}}$ denote by the set of indices of contact candidate nodes, and let $n_{\mathrm{c}} = |\mathcal{P}_{\mathrm{c}}|$. We assume that the obstacle, or rigid surface, corresponding to each contact candidate node is to be known. More precisely, for each $p \in \mathcal{P}_{\mathrm{c}}$, the interior of the corresponding obstacle in the dim-dimensional ($\mathrm{dim} \in \{2, 3\}$) space is identified by

$$\left\{ \boldsymbol{x} \in \mathbb{R}^{\mathrm{dim}} \mid \varphi^p(\boldsymbol{x}) > 0 \right\},$$

where $\boldsymbol{x}$ is the position vector with respect to a fixed orthonormal reference frame, and the given function $\varphi^p : \mathbb{R}^{\mathrm{dim}} \to \mathbb{R}$ is assumed to be twice continuously differentiable. We deal with only possible contact between a candidate node and the corresponding obstacle, and the self-contact of the elastic body is not considered.

At the deformed state corresponding to $\boldsymbol{u}$, we denote by $\boldsymbol{x}^p(\boldsymbol{u}) \in \mathbb{R}^{\mathrm{dim}}$ the position vector of the pth node with respect to the reference frame. Then the admissible set of $\boldsymbol{u}$ is given by

$$\left\{ \boldsymbol{u} \in \mathbb{R}^d \mid \varphi^p(\boldsymbol{x}^p(\boldsymbol{u})) \leq 0 \ (p \in \mathcal{P}_{\mathrm{c}}) \right\}.$$

We may assume without loss of generality that φ^p satisfies $\|\nabla \varphi^p(\boldsymbol{x})\| = 1$ on $\{\boldsymbol{x} \in \mathbb{R}^{\mathrm{dim}} \mid \varphi^p(\boldsymbol{x}) = 0\}$. Then, at a point $\boldsymbol{x}$ on the obstacle we see that the vector

$$\boldsymbol{n}^p(\boldsymbol{x}) = \nabla \varphi^p(\boldsymbol{x})$$

corresponds to the unit inner normal vector as illustrated in Figure 1.

Define $\boldsymbol{\phi} : \mathbb{R}^d \to \mathbb{R}^{n_{\mathrm{c}}}$ by

$$\boldsymbol{\phi}(\boldsymbol{u}) = \left(\varphi^1(\boldsymbol{x}^1(\boldsymbol{u})), \ldots, \varphi^{n_{\mathrm{c}}}(\boldsymbol{x}^{n_{\mathrm{c}}}(\boldsymbol{u})) \right)^{\mathrm{T}}.$$

The non-penetration condition is written as

$$\boldsymbol{g} := -\boldsymbol{\phi}(\boldsymbol{u}) \geq \boldsymbol{0},$$

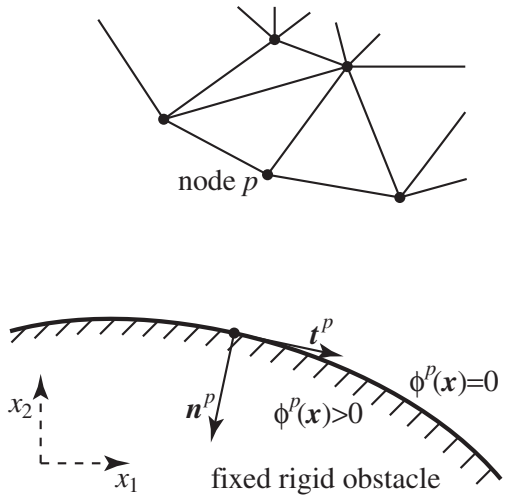

Figure 1: Contact candidate node p with the curved obstacle φ^p.

where g_p corresponds to the nodal gap.

The frictionless assumption implies that the contact reaction force at each candidate node acts in the normal direction of the rigid surface. We denote by r_p such a reaction force at the pth node, and then the reaction force vector is written as $r_p \boldsymbol{n}^p(\boldsymbol{x}^p(\boldsymbol{u}))$. From the unilateral contact assumption we have $r_p \leq 0$, which means the no-adhesion condition. By using the definition of $\boldsymbol{\phi}$, the vector of generalized reactions is given by $\nabla\boldsymbol{\phi}(\boldsymbol{u})^{\mathrm{T}}\boldsymbol{r}$.

Consequently, our problem is to find the continuation of the solution $(\boldsymbol{u}, \boldsymbol{r}, \lambda)$ to the mixed complementarity problem

$$\nabla\pi(\boldsymbol{u}) = \lambda \boldsymbol{f} + \nabla\boldsymbol{\phi}(\boldsymbol{u})^{\mathrm{T}}\boldsymbol{r}, \tag{9}$$

$$\boldsymbol{g} = -\boldsymbol{\phi}(\boldsymbol{u}), \tag{10}$$

$$g_p \geq 0, \quad r_p \leq 0, \quad g_p r_p = 0, \qquad p = 1, \ldots, n_{\mathrm{c}}. \tag{11}$$

3 Implicit reformulation of complementarity conditions

Let $\psi_{\mathrm{FB}} : \mathbb{R}^2 \to \mathbb{R}$ denote the Fischer–Burmeister function defined by

$$\psi_{\mathrm{FB}}(a, b) = \sqrt{a^2 + b^2} - (a + b).$$

It is known that ψ_{FB} satisfies

$$\psi_{\mathrm{FB}}(a, b) = 0 \quad \Leftrightarrow \quad a \geq 0, \quad b \geq 0, \quad ab = 0.$$

Define $\psi : \mathbb{R}^3 \to \mathbb{R}$ by

$$\psi(a, b, \rho) = \sqrt{a^2 + b^2 + 2\rho^2} - (a + b), \tag{12}$$

which is the smoothed Fischer–Burmeister function proposed in [16] for solving linear complementarity problems.

Proposition 3.1. *$\psi(a, b, \rho) = 0$ if and only if*

$$a \geq 0, \quad b \geq 0, \quad ab = \rho^2. \tag{13}$$

Proof. It is easy to see that (13) implies $\psi(a, b, \rho) = 0$. Conversely, suppose $\psi(a, b, \rho) = 0$. We have

$$a + b = \sqrt{a^2 + b^2 + 2\rho^2}. \tag{14}$$

Squaring both sides of (14) yields

$$ab = \rho^2. \tag{15}$$

Moreover, we obtain $a + b \geq 0$ and $ab \geq 0$ from (14) and (15), respectively, and hence a, $b \geq 0$. Consequently, (13) is satisfied. □

Let η_1, $\eta_2 : \mathbb{R} \to \mathbb{R}$ be smooth functions satisfying the following property:

Assumption 3.2. *The equation $\eta_1(c^2) = \eta_2(c)$ has the unique solution at $c = 0$.*

Proposition 3.3. *Suppose that Assumption 3.2 is satisfied. Then $\boldsymbol{y}$, $\boldsymbol{z} \in \mathbb{R}^n$ and $\rho \in \mathbb{R}$ satisfy*

$$\psi(y_i, z_i, \rho) = 0, \qquad i = 1, \ldots, n, \tag{16}$$

$$\eta_1(\boldsymbol{y}^{\mathrm{T}}\boldsymbol{z}/n) = \eta_2(\rho) \tag{17}$$

if and only if

$$\boldsymbol{y} \geq \boldsymbol{0}, \quad \boldsymbol{z} \geq \boldsymbol{0}, \quad \boldsymbol{y}^{\mathrm{T}}\boldsymbol{z} = 0, \quad \rho = 0. \tag{18}$$

Proof. It is easy to show that (16) and (17) hold if (18) is satisfied. Conversely, suppose (16) and (17). If $\rho = 0$, then (18) follows immediately from Proposition 3.1. Hence, it remains to show that (16) and (17) imply $\rho = 0$. It follows from Proposition 3.1 that (16) implies $y_i z_i = \rho^2$ $(i = 1, \ldots, n)$. Hence, we obtain

$$\boldsymbol{y}^{\mathrm{T}}\boldsymbol{z}/n = \rho^2. \tag{19}$$

Substituting (19) into (17) yields $\eta_1(\rho^2) = \eta_2(\rho)$, from which and Assumption 3.2 we obtain $\rho = 0$. □

It follows from Proposition 3.3 that (9)–(11) is equivalently rewritten as

$$\nabla\pi(\boldsymbol{u}) = \lambda\boldsymbol{f} + \nabla\boldsymbol{\phi}(\boldsymbol{u})^{\mathrm{T}}\boldsymbol{r}, \tag{20}$$

$$\boldsymbol{g} = -\boldsymbol{\phi}(\boldsymbol{u}), \tag{21}$$

$$\psi(g_p, -r_p, \rho) = 0, \qquad p = 1, \ldots, n_{\mathrm{c}}, \tag{22}$$

$$\eta_1(-\boldsymbol{g}^{\mathrm{T}}\boldsymbol{r}/n_{\mathrm{c}}) = \eta_2(\rho), \tag{23}$$

where $\boldsymbol{u}$, $\boldsymbol{g}$, $\boldsymbol{r}$, and ρ are the variables.

Our basic idea is to solve (20)–(23) by using a conventional Newton method for smooth nonlinear equations. Note that the left-hand side of (22) is continuously differentiable at any point except $(g_p, r_p, \rho) = \boldsymbol{0}$. Since the set of such non-differentiable points, $\{(\boldsymbol{u}, \boldsymbol{g}, \boldsymbol{r}, \rho) \mid \exists\check{p} : g_{\check{p}} = r_{\check{p}} = \rho = 0\}$,

has measure zero, with probability one (22) is continuously differentiable at an intermediate solution attained by the Newton method.

It is emphasized that the smoothing parameter ρ is considered as an independent variable in (20)–(23). Roughly speaking, $|\rho|$ indicates the 'level' of smoothing, which is adjusted automatically to the residual of the complementarity conditions, $\boldsymbol{g}^{\mathrm{T}}\boldsymbol{r}$, as discussed in Remark 4.4 below. As the residual of a given initial point is larger, the initial value for ρ is chosen so that its absolute value is larger. As the residual becomes smaller, $|\rho|$ automatically becomes smaller. Thus, ρ is not treated as an outer parameter controlled irrespective of the solution at each Newton step but as a variable in the nonlinear equations in our approach, which distinguishes our method from conventional smoothing methods, non-interior point methods, and interior-point methods in the literature.

4 Warm-start approach via implicit formulation

We trace the equilibrium path numerically in a stepwise manner, by continuing from a known solution $(\boldsymbol{u}^k, \boldsymbol{r}^k, \lambda^k)$ to a new solution $(\boldsymbol{u}^{k+1}, \boldsymbol{r}^{k+1}, \lambda^{k+1})$ along the path. Let

$$\Delta\boldsymbol{u} = \boldsymbol{u}^{k+1} - \boldsymbol{u}^k,$$
$$\Delta\lambda = \lambda^{k+1} - \lambda^k.$$

In the following, we distinguish the quantities evaluated at the kth loading step k by superscript k, while those at the $(k+1)$th step are not marked explicitly, unless it is not clear from the context.

4.1 Discretized governing equations for arc-length method

We use the scheme of conventional arc-length methods in order to deal with limit points of the load factor along the equilibrium path [3]. We regard λ as an additional variable by considering the additional constraint condition

$$\|(\Delta\boldsymbol{u}, \boldsymbol{r}, \Delta\lambda)\|_H = \bar{\theta},$$

where H and $\bar{\theta} > 0$ are a given matrix and constant scalar, respectively, and $\|\cdot\|_H$ is the generalized vector norm defined with the given matrix H as $\|\boldsymbol{\xi}\|_H = \|H\boldsymbol{\xi}\|_2$.

Consequently, the system of governing equations, (9)–(11), is discretized as

$$\nabla\pi(\boldsymbol{u}^k + \Delta\boldsymbol{u}) = (\lambda^k + \Delta\lambda)\boldsymbol{f} + \nabla\boldsymbol{\phi}(\boldsymbol{u}^k + \Delta\boldsymbol{u})^{\mathrm{T}}\boldsymbol{r}, \tag{24}$$
$$\boldsymbol{g} = -\boldsymbol{\phi}(\boldsymbol{u}^k + \Delta\boldsymbol{u}), \tag{25}$$
$$g_p \geq 0, \quad r_p \leq 0, \quad g_p r_p = 0, \qquad p = 1, \ldots, n_{\mathrm{c}}, \tag{26}$$
$$\|(\Delta\boldsymbol{u}, \boldsymbol{r}, \Delta\lambda)\|_H = \bar{\theta}, \tag{27}$$

where $\Delta\boldsymbol{u}$, $\boldsymbol{r}$, $\boldsymbol{g}$, and $\Delta\lambda$ are the unknown variables. Typically, we simply choose H in (27) as $\|(\Delta\boldsymbol{u}, \boldsymbol{r}, \Delta\lambda)\|_H = \|(\Delta\boldsymbol{u}, \Delta\lambda)\|_2$.

4.2 Implicit nonlinear equations

Besides Assumption 3.2 we impose a further restriction to η_1 and η_2 as follows.

Assumption 4.1. *$c = 0$ is a nondegenerate solution of $\eta_1(c^2) = \eta_2(c)$.*

Assumption 4.1 is equivalent to the regularity condition of the Jacobian, i.e. $\mathrm{d}\eta_1(c^2)/\mathrm{d}c \neq \mathrm{d}\eta_2(c)/\mathrm{d}c$ at $c = 0$ [24, Chap. 11]. As discussed in detail in Remark 4.2 below, Assumption 4.1 is necessary to ensure a fast local convergence property in the solution.

For a constant $\gamma \in]0, 1]$, let

$$\eta_1(c) = \gamma^2 c + 1, \quad \eta_2(c) = e^{\gamma c}, \tag{28}$$

which satisfy Assumption 3.2 and Assumption 4.1. By using (28) we reformulate the complementarity problem (24)–(27) into a system of nonlinear equations which is to be solved by using a conventional Newton method. It follows from Proposition 3.3 that (24)–(27) are equivalent to

$$\nabla\pi(\boldsymbol{u}^k + \Delta\boldsymbol{u}) - (\lambda^k + \Delta\lambda)\boldsymbol{f} - \nabla\boldsymbol{\phi}(\boldsymbol{u}^k + \Delta\boldsymbol{u})^{\mathrm{T}}\boldsymbol{r} = \boldsymbol{0}, \tag{29}$$

$$\boldsymbol{g} + \boldsymbol{\phi}(\boldsymbol{u}^k + \Delta\boldsymbol{u}) = \boldsymbol{0}, \tag{30}$$

$$\psi(g_p, -r_p, \rho) = 0, \qquad p = 1, \ldots, n_{\mathrm{c}}, \tag{31}$$

$$-\gamma^2\boldsymbol{g}^{\mathrm{T}}\boldsymbol{r} - n_{\mathrm{c}}(e^{\gamma\rho} - 1) = 0, \tag{32}$$

$$\|(\Delta\boldsymbol{u}, \boldsymbol{r}, \Delta\lambda)\|_H^2 - \bar{\theta}^2 = 0, \tag{33}$$

which is our goal formulation. Note that the system of equations (29)–(33) consists of $(d + 2n_{\mathrm{c}} + 2)$ equations in the same number of unknown variables $\Delta\boldsymbol{u}$, $\boldsymbol{r}$, $\boldsymbol{g}$, $\Delta\lambda$, and ρ.

Remark 4.2. For an implicit reformulation it is sufficient that η_1 and η_2 satisfy Assumption 3.2 as discussed in section 2. For example, a pair of

$$\eta_1(c) = c/2, \quad \eta_2(c) = c^2, \tag{34}$$

satisfies Assumption 3.2, which implies that (32) can be replaced with

$$-\boldsymbol{g}^{\mathrm{T}}\boldsymbol{r} - 2n_{\mathrm{c}}\rho^2 = 0$$

without changing the solution. As a solution technique we attempt to solve the obtained nonlinear equations by using a conventional Newton method. In this procedure Assumption 3.2 is required to ensure a fast local convergence of the Newton method [24, Chap. 11]. Indeed, in section 5.1 we will show through numerical experiments that for the implicit formulation with (34) the Newton method converges to the solution only with a linear convergence property.

Another example satisfying Assumption 3.2 and Assumption 4.1 is the pair of

$$\eta_1(c) = c, \quad \eta_2(c) = c + c^3, \tag{35}$$

which yields

$$-\boldsymbol{g}^{\mathrm{T}}\boldsymbol{r} - n_{\mathrm{c}}(\rho + \rho^3) = 0$$

instead of (32). Numerical experiments in section 5.1 demonstrate that the both implicit formulations with (28) and (35) can enjoy a fast local convergence property of the Newton method. ■

As discussed in section 4.3 below in detail, γ plays a role of the scaling parameter to obtain the initial solution satisfying the warm start condition. Suppose that $\boldsymbol{g}_{(0)}$ and $\boldsymbol{r}_{(0)}$ are given as the initial values for $\boldsymbol{g}$ and $\boldsymbol{r}$, respectively. If

$$\boldsymbol{g}_{(0)}^{\mathrm{T}}\boldsymbol{r}_{(0)} < n_{\mathrm{c}} \tag{36}$$

is satisfied, then we simply set $\gamma = 1$. Then we choose an initial value $\rho_{(0)}$ for ρ so that (32) with $\gamma = 1$ is satisfied. If $\boldsymbol{g}_{(0)}$ and $\boldsymbol{r}_{(0)}$ do not satisfy (36), then the equation $-\boldsymbol{g}_{(0)}^{\mathrm{T}}\boldsymbol{r}_{(0)} = n_{\mathrm{c}}(e^{\rho_{(0)}} - 1)$ in the variable $e^{\rho_{(0)}}$ does not have a solution. We relax the condition (36) as

$$\boldsymbol{g}_{(0)}^{\mathrm{T}}\boldsymbol{r}_{(0)} < n_{\mathrm{c}}(1 - \underline{\gamma})$$

in order to avoid that too small value is assigned as $\rho_{(0)}$, where $\underline{\gamma} \in]0, 1[$ is a constant tolerance, e.g. $\underline{\gamma} = 10^{-2}$. Conversely, if $\boldsymbol{g}_{(0)}^{\mathrm{T}}\boldsymbol{r}_{(0)} \geq n_{\mathrm{c}}(1 - \underline{\gamma})$, then we choose γ so that

$$\gamma^2 \boldsymbol{g}_{(0)}^{\mathrm{T}}\boldsymbol{r}_{(0)} = n_{\mathrm{c}}(1 - \underline{\gamma})$$

is satisfied, and choose $\rho_{(0)}$ so that (32) is satisfied. Thus, we define γ by

$$\gamma = \begin{cases} 1 & \text{if } \boldsymbol{g}_{(0)}^{\mathrm{T}}\boldsymbol{r}_{(0)} < n_{\mathrm{c}}(1 - \underline{\gamma}), \\ \left[n_{\mathrm{c}}(1 - \underline{\gamma}) / (\boldsymbol{g}_{(0)}^{\mathrm{T}}\boldsymbol{r}_{(0)}) \right]^{1/2} & \text{if } \boldsymbol{g}_{(0)}^{\mathrm{T}}\boldsymbol{r}_{(0)} \geq n_{\mathrm{c}}(1 - \underline{\gamma}), \end{cases} \tag{37}$$

which guarantees that (32) has a solution, $\rho_{(0)}$, for any $\boldsymbol{g}_{(0)}$ and $\boldsymbol{r}_{(0)}$.

4.3 Warm start condition

In the process of arc-length method we solve (29)–(33) successively from a known equilibrium state $(\boldsymbol{u}^k, \boldsymbol{g}^k, \boldsymbol{r}^k, \lambda^k)$ at the kth loading stage to a new solution $(\Delta\boldsymbol{u}^k, \boldsymbol{g}^{k+1}, \boldsymbol{r}^{k+1}, \Delta\lambda^k)$ corresponding to the $(k+1)$th loading stage. In many cases we may expect that there exists only small perturbation of the governing equations (29)–(33) from the kth stage to the $(k+1)$th stage. Hence, it is natural to expect that the solution

$$\Delta\boldsymbol{u}^{k-1}, \quad \boldsymbol{g}^k, \quad \boldsymbol{r}^k, \quad \Delta\lambda^{k-1}$$

at the previous stage is considerably close to the solution at the current stage, and hence we aim at exploiting the previous solution to construct an initial point which may be expected to satisfy a warm start condition.

We propose to assign an initial solution for solving (29)–(33) as follows. Firstly, we simply use the previous solution as the initial values for $\Delta\boldsymbol{u}$, $\boldsymbol{r}$, and $\Delta\lambda$, i.e.

$$\Delta\boldsymbol{u}_{(0)} := \Delta\boldsymbol{u}^{k-1}, \tag{38}$$

$$\boldsymbol{r}_{(0)} := \boldsymbol{r}^k, \tag{39}$$

$$\Delta\lambda_{(0)} := \Delta\lambda^{k-1}. \tag{40}$$

Then the initial value for $\boldsymbol{g}$ is naturally given by

$$\boldsymbol{g}_{(0)} := -\boldsymbol{\phi}(\boldsymbol{u}^k + \Delta\boldsymbol{u}_{(0)}). \tag{41}$$

We next compute the scaling parameter γ by substituting $\boldsymbol{g}_0$ and $\boldsymbol{r}_0$ into (37). Finally, it is natural to choose the initial value, $\rho_{(0)}$, for ρ so that

$$\eta_1(-\boldsymbol{g}_{(0)}^{\mathrm{T}}\boldsymbol{r}_{(0)}/n_{\mathrm{c}}) = \eta_2(\rho_{(0)})$$

is satisfied. Explicitly we give $\rho_{(0)}$ by

$$\rho_{(0)} := \begin{cases} \rho^* & \text{if } |\rho^*| > \underline{\rho}, \\ \underline{\rho} & \text{otherwise}, \end{cases} \tag{42}$$

$$\rho^* = \frac{1}{\gamma}\log\left(1 - \frac{\gamma}{n_{\mathrm{c}}}\boldsymbol{g}_{(0)}^{\mathrm{T}}\boldsymbol{r}_{(0)}\right), \tag{43}$$

where $\underline{\rho} > 0$ is a small constant, e.g. $\underline{\rho} = 10^{-3}$, in order to ensure the smoothing of Fischer–Burmeister function at the initial point. Note again that γ is a scaling parameter with which the right-hand side of (42) is always well-defined.

It is emphasized that the initial point $(\Delta\boldsymbol{u}_{(0)}, \boldsymbol{r}_{(0)}, \boldsymbol{g}_{(0)}, \Delta\lambda_{(0)}, \rho_{(0)})$ defined by (38)–(42) satisfies (30), (32), and (33), and hence it is regarded as a good initial point for solving the system (29)–(33) so that the conventional Newton method can enjoy the warm start condition.

Remark 4.3. As discussed in Remark 4.2, we can obtain an alternative implicit formulation by using (35) instead of (28). In that case, the initial value $\rho_{(0)}$ compatible with $\boldsymbol{g}_{(0)}$ and $\boldsymbol{r}_{(0)}$ may be obtained by solving a nonlinear equation

$$-\boldsymbol{g}_{(0)}^{\mathrm{T}}\boldsymbol{r}_{(0)} - n_{\mathrm{c}}(\rho_{(0)} + \rho_{(0)}^3) = 0 \tag{44}$$

instead of (42). However, we prefer not to solve an additional nonlinear equation (44) numerically to find an initial point, which is the reason why we present the formulation yielded by (35). ■

Remark 4.4. The role of ρ can be captured more clearly by rewriting (32) as

$$\rho = \frac{1}{\gamma}\log\left(-\frac{\gamma}{n_{\mathrm{c}}}\boldsymbol{g}^{\mathrm{T}}\boldsymbol{r} + 1\right),$$

from which we may regard ρ as a measure of the residual of the complementarity conditions, $-\boldsymbol{g}^{\mathrm{T}}\boldsymbol{r} = 0$. Since we define $\rho_{(0)}$ by (42), as the residual $|\boldsymbol{g}_{(0)}^{\mathrm{T}}\boldsymbol{r}_{(0)}|$ at the initial point is larger, we choose $\rho_{(0)}$ such that $|\rho_{(0)}|$ is larger. This means that we assign a large value to the smoothing parameter ρ for a 'cold start' problem in order to avoid numerical instabilities which may possibly arise from the nonsmoothness of the Fischer–Burmeister function. In the procedure of the Newton method we may expect that the residual $|\boldsymbol{g}^{\mathrm{T}}\boldsymbol{r}|$ decreases gradually, because $\boldsymbol{g}^{\mathrm{T}}\boldsymbol{r} = 0$ should be satisfied at the solution of (29)–(33). As the residual $|\boldsymbol{g}^{\mathrm{T}}\boldsymbol{r}|$ becomes smaller, ρ automatically approaches zero. This mechanism also helps to prevent the Newton method to hitting an intermediate solution at which (31) is not continuously differentiable, because in most cases $\boldsymbol{g}^{\mathrm{T}}\boldsymbol{r} \neq 0$ at an intermediate solution and hence $\rho \neq 0$ is expected. ■

Remark 4.5. As discussed in Remark 4.4 the auxiliary variable ρ in our formulation is regarded as a measure of the residual of the complementarity conditions. Alternatively we may choose

$$\rho = -\frac{1}{n_{\mathrm{c}}}\boldsymbol{g}^{\mathrm{T}}\boldsymbol{r} \tag{45}$$

as a measure of the residual, which is yielded by

$$\eta_1(c) = c, \quad \eta_2(c) = c. \tag{46}$$

Indeed, many path-following methods for complementarity problems, e.g. [17, 36, 37, 39], are designed based on

$$\rho = -g_p r_p, \quad p = 1, \ldots, n_{\mathrm{c}}, \tag{47}$$

which implies (45). Here, $\rho > 0$ is not considered as a variable but as a constant parameter, which is decreased gradually to zero. However, (45) is not accepted in our implicit formulation, because η_1 and η_2 in (46) does not satisfy Assumption 3.2. ■

Remark 4.6. The initial point constructed by (38)–(42) is not an interior point in general, and hence it is not easy to exploit a warm start condition of this point with the interior-point method. This motivates us to develop a non-interior point method. ■

4.4 Detection of nonsmooth equilibrium point

Along the equilibrium path there exists a point at which the set of contact nodes changes. In general, such a point corresponds to a nonsmooth point on the equilibrium path. Based on the formulation (29)–(33), we show that such a nonsmooth point can be computed easily.

Firstly, we compare the kth and $(k+1)$th equilibrium states computed in order to check whether there exists a node whose contact condition changes in the interval, i.e. the condition changes either from on contact to free or from free to on contact. If exists, we denote by $\hat{p}$ the index of such a node. The nonsmooth point associated with the $\hat{p}$th node is characterized by $g_{\hat{p}} = r_{\hat{p}} = 0$. This relation can be replaced with a equation

$$g_{\hat{p}} - r_{\hat{p}} = 0, \tag{48}$$

because the complementarity condition, $g_{\hat{p}} r_{\hat{p}} = 0$, is always required to hold. Consequently, the nonsmooth point is found by solving the following system of nonlinear equations:

$$\nabla\pi(\boldsymbol{u}^k + \Delta\boldsymbol{u}) - (\lambda^k + \Delta\lambda)\boldsymbol{f} - \nabla\boldsymbol{\phi}(\boldsymbol{u}_k + \Delta\boldsymbol{u})^{\mathrm{T}}\boldsymbol{r} = \boldsymbol{0}, \tag{49}$$

$$\boldsymbol{g} + \boldsymbol{\phi}(\boldsymbol{u}_k + \Delta\boldsymbol{u}) = \boldsymbol{0}, \tag{50}$$

$$\phi(g_p, -r_p, \rho) = 0, \qquad \forall p = 1, \ldots, n_{\mathrm{c}}, \tag{51}$$

$$-\gamma\boldsymbol{g}^{\mathrm{T}}\boldsymbol{r} - n_{\mathrm{c}}(e^{\gamma\rho} - 1) = 0, \tag{52}$$

$$g_{\hat{p}} - r_{\hat{p}} = 0. \tag{53}$$

Then we solve (49)–(53) by using a conventional Newton method, as in the case of a usual step of the arc-length method. Compared to (29)–(33), the constraint condition on the arc-length, (33), is replaced with the degenerate condition of the pth complementarity condition, (53).

In section 5.2 and section 5.3 we illustrate through numerical examples that we can find nonsmooth limit points of the load factor by solving (49)–(53).

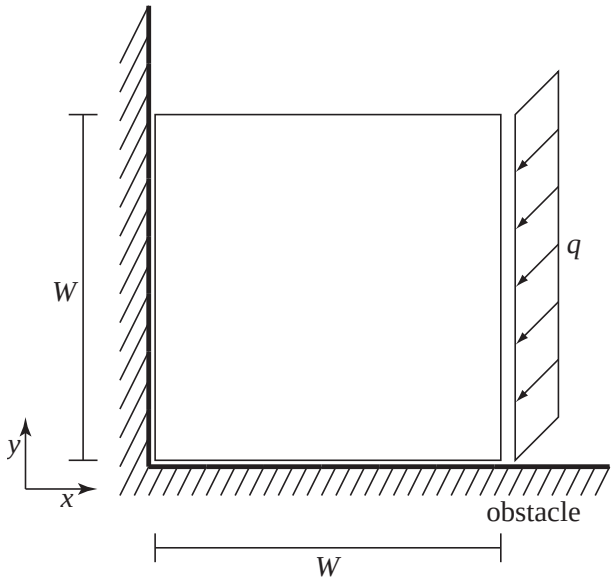

Figure 2: A square elastic block on the obstacle.

5 Numerical experiments

Frictionless contact problems are solved by using the arc-length method with the warm start condition described in section 4. In the numerical experiments we choose the parameters as $\underline{\gamma} = 10^{-2}$ in (37) and $\underline{\rho} = 10^{-3}$ in (42). Computation has been carried out on Core2 Duo P8400 (2.26 GHz with 4.0 GB memory) with MATLAB R2008b [34].

5.1 Linear elastic body

In this section we solve a small deformation problem with the cold start condition of a given initial point in order to demonstrate that our formulation can enjoy a fast local convergence property and a global convergence property when a conventional method for smooth nonlinear equations is applied.

Consider an isotropic linear elastic body in the plane stress as shown in Figure 2, where its thickness is 10 mm and $W = 2$ m. The elastic modulus and Poisson's ratio are taken to be 100 MPa and 0.3, respectively. The solid is discretized into 50×50 four-node quadrilateral (Q4) elements. All the nodes on the left and lower boundaries are supposed to be contact candidates, and be in contact with the obstacles without reactions. The right boundary is subjected to the uniformly distributed load consisting of 0.5 MPa in the negative directions of the x- and y-axes.

We solve some different formulations for this problem by using a MATLAB built-in function `fsolve`, which is a conventional trust-region dogleg method with `'TolFun'`$= 10^{-7}$ and otherwise the default settings. (20)–(23), where $\boldsymbol{\phi}$ is a linear function. Figure 3 illustrates the obtained equilibrium configuration. To compare the convergence properties, we consider four cases:

- Case 1: (20)–(23) with $\eta_1(c) = \gamma^2 c + 1$ and $\eta_2(c) = e^{\gamma c}$;
- Case 2: (20)–(23) with $\eta_1(c) = c$ and $\eta_2(c) = c + c^3$;
- Case 3: (20)–(23) with $\eta_1(c) = c/2$ and $\eta_2(c) = c^2$;

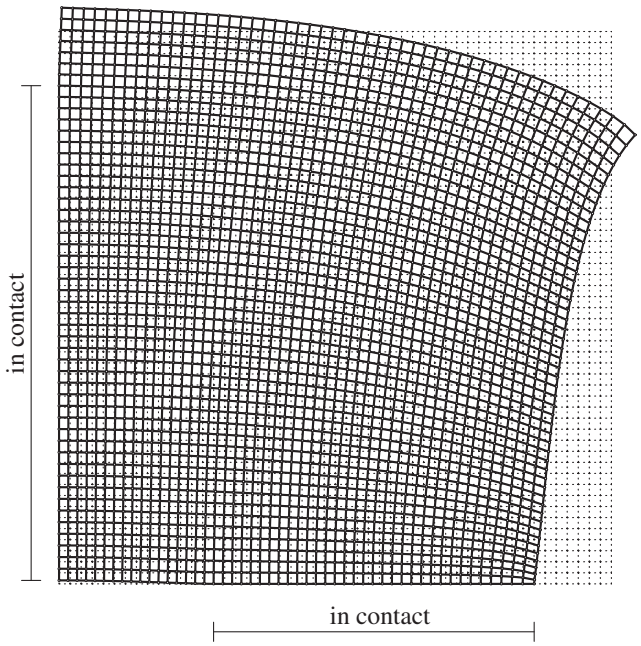

Figure 3: Deformed configuration of the square elastic body at the equilibrium state (displacements amplified 10 times).

- Case 4: (20)–(22) with $\rho = 0$.

Here, Case 1 corresponds to the formulation proposed in section 4 for large deformations. We see that η_1 and η_2 in Case 1, Case 2, and Case 3 satisfy Assumption 3.2, while Assumption 4.1 is satisfied only in Case 1 and Case 2 (see Remark 4.2). Case 4 corresponds to the nonsmooth equations formulation based on the Fischer–Burmeister function without smoothing.

In order to examine the cold start condition, we give an initial point for the trust-region method by $\boldsymbol{u}_{(0)} = \mathbf{0}$, $\boldsymbol{g}_{(0)} = -\mathbf{1}$, and $\boldsymbol{r}_{(0)} = \mathbf{1}$. We obtain $\gamma = 1$ from (37) and $\rho_{(0)} = 0.6931$ from (42) in Case 1. For $\rho_{(0)}$ in Case 2 we solve the nonlinear equation $\boldsymbol{g}_{(0)}^{\mathrm{T}}\boldsymbol{r}_{(0)}/n_{\mathrm{c}} = \rho_{(0)} + \rho_{(0)}^3$ to find $\rho_{(0)} = 0.6823$. In Case 3, we put $\rho_{(0)} = 0.7071$ which is obtained from $\boldsymbol{g}_{(0)}^{\mathrm{T}}\boldsymbol{r}_{(0)}/(2n_{\mathrm{c}}) = \rho_{(0)}^2$. Consequently, Case 1, Case 2, and Case 3 share the same residuals at their initial points. However, in Case 3 the trust region method does not converge within 1000 iterations. The initial point in Case 4 consists of $\boldsymbol{u}_{(0)}$, $\boldsymbol{g}_{(0)}$, and $\boldsymbol{r}_{(0)}$ defined above, because ρ is not a variable but is always equal to zero. It is emphasized that those initial points are not interior points.

Figure 4 illustrates the convergence history of the sum-of-squares of the residuals of the nonlinear equations. The CPU time required in Case 1 is 50.4 sec. Note again that the algorithm fails to converge in Case 3 from the initial point given above. Hence, in Figure 4 we show the result from another initial point which is sufficiently near from the solution for comparison of local convergence properties. It is observed from Figure 4 that Case 1 and Case 2 enjoy fast local convergence in the neighborhood of the solution as expected (see Remark 4.2), while Case 3, which does not satisfy Assumption 4.1, has a linear convergence property. Although Case 4 also has a fast local convergence property, the number of iterations required in Case 4 is very large compared with Case 1 or Case 2. This confirms that using the smoothing scheme of the Fischer–Burmeister function decreases the number of iterations drastically.

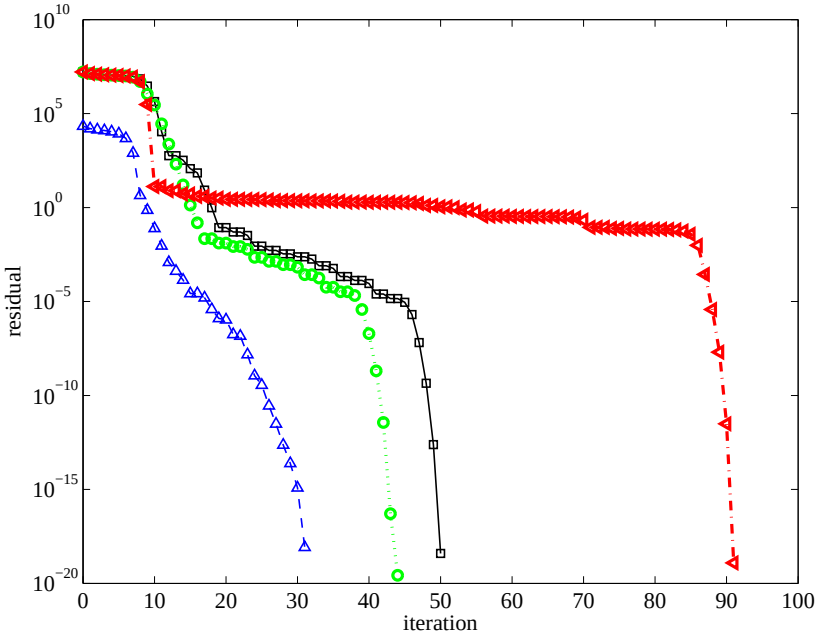

Figure 4: Convergence histories of the sum-of-squares of the residuals in the trust-region dogleg method for different η_1 and η_2. '□': Case 1, $\eta_1(c) = \gamma^2 c + 1$, $\eta_2(c) = e^{\gamma c}$ with $\gamma = 1$; '○': Case 2, $\eta_1(c) = c$, $\eta_2(c) = c + c^3$; '△': Case 3, $\eta_1(c) = c/2$, $\eta_2(c) = c^2$ (an initial point near the solution is given); '◁': Case 4, a nonsmooth formulation using the Fischer–Burmeister function.

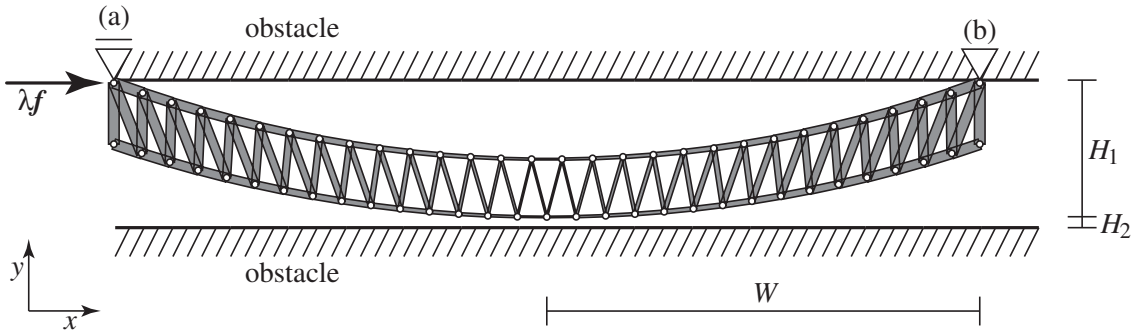

Figure 5: A plane arch truss with flat obstacles.

5.2 Large deformation with flat obstacles

In this and the following sections we solve large deformation problems of linear elastic trusses in order to demonstrate that our warm-start strategy reduces the number of iterations of each loading step in the arc-length method. At almost all loading steps a conventional Newton method converges to the solution within four iterations, and in some cases it finds the solution in two iterations. We solve the system of nonlinear equations (29)–(33) by using `csolve` [33], which is an improvement of the MATLAB built-in function `fsolve` and based on the quasi-Newton method with BFGS update of the inverse of Hessian.

Consider a plane arch shown in Figure 5, where $W = 7.5\,\mathrm{m}$, $H_1 = 2.3225\,\mathrm{m}$, and $H_2 = 0.1\,\mathrm{m}$.

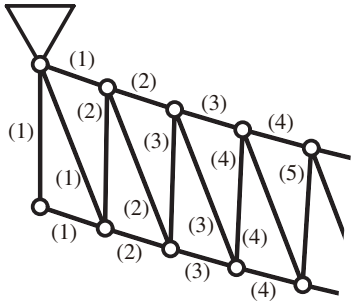

Figure 6: A plane arch truss with flat obstacles.

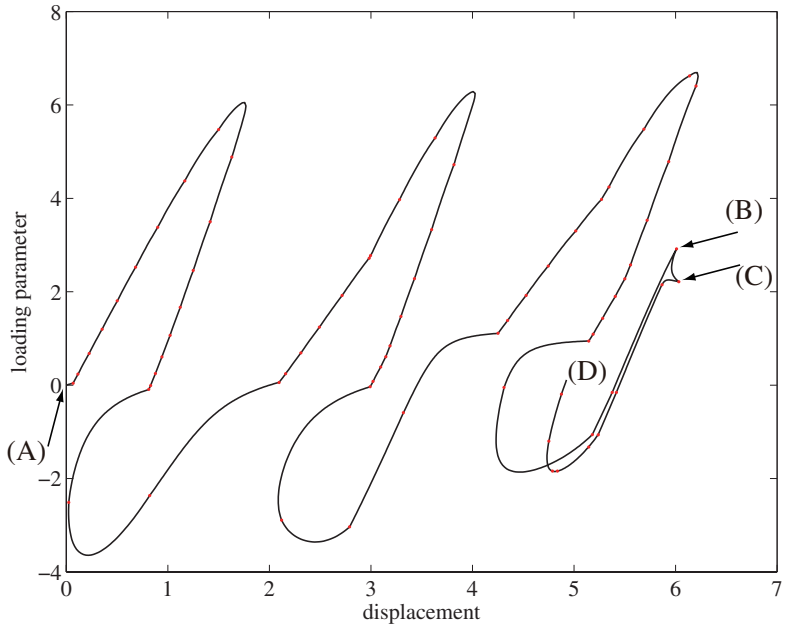

Figure 7: Equilibrium path of the plane truss with flat obstacles.

The truss consists of 61 nodes located on two circles sharing the common centers. The nodes of the upper layer are located on the circle with the half open angle $\omega = 20\,\mathrm{deg}$ and the radius $W/\sin\omega\,(\mathrm{m})$. The nodes of the lower layer are located on the circle with the same center and the radius $(W/\sin\omega) + 1\,(\mathrm{m})$. The displacement of the node (a) in the y-direction is constrained, while the node (b) is pin-supported, and hence $d = 119$. The truss is located between two rigid obstacles with horizontal flat surfaces, where the nodes (a) and (b) are on the upper one.

Since the nodes of the lower layer may also contact with the upper obstacle, we consider $n_{\mathrm{c}} = 31 \times 2 + 28 = 90$ contact candidates. The geometrical nonlinearity is considered by using the Biot strain. The proportional load $5\lambda\,(\mathrm{kN})$ is applied at the node (a) in the x-direction. The arc-length constraint is given by $\|(\Delta \boldsymbol{u}, \Delta\lambda)\|_2 = \bar{\theta}$ with $\bar{\theta} = 0.1$. The elastic modulus is $20\,\mathrm{GPa}$. The cross-sectional areas of members in groups (1), (2), (3), (4), $\ldots$ shown in Figure 6 are given as $0.33\,\mathrm{m}^2$, $0.31\,\mathrm{m}^2$, $0.29\,\mathrm{m}^2$, $0.27\,\mathrm{m}^2, \ldots$, respectively.

The obtained equilibrium path is plotted in Figure 7, which shows the variation (A)$\rightarrow$(B)$\rightarrow$(C)$\rightarrow$(D)

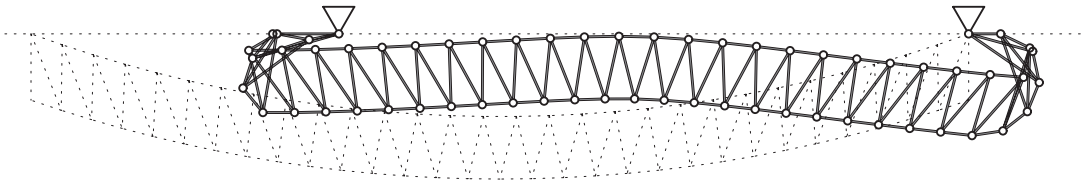

Figure 8: Deformed configuration (solid line) of the plane truss with flat obstacles at the equilibrium state (D) in Figure 7; dotted line: undeformed configuration.

Table 1: Number of iterations required at each loading step of the plane truss with flat obstacles.

# of iterations	2	3	4	5	6	7	8	9	$10 \leq n \leq 16$
frequency	273	836	139	79	26	8	2	1	5

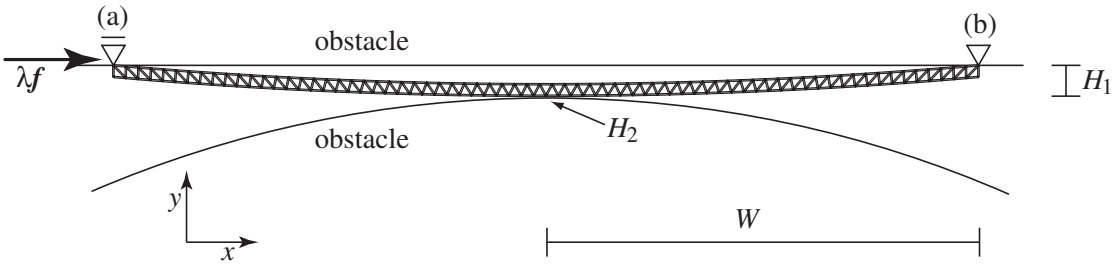

Figure 9: A plane arch truss with curved obstacles.

of the loading parameter λ with respect to the displacement of the node (a). Along the equilibrium path 129 nonsmooth points are found by using the method presented in section 4.4.

Figure 8 depicts the deformed configuration at the equilibrium state (D) in Figure 7. Since (D) exists beyond the bifurcation point (C), the configuration at (D) is not symmetric, while all the configurations between (A) and (C) are symmetric. It is observed that the equilibrium state (B) is an angular limit point due to a change of contact conditions.

The number of iterations required at each loading step is listed in Table 1, which means, e.g., the solution is found with two iterations in 273 loading stages. We can see that the Newton method converges within four iterations at almost all loading steps. Thus, in many cases, the solution at the previous loading step can be used as a good initial point for the current step to solve our implicit formulation.

5.3 Large deformation with curved obstacles

Consider a linear truss shown in Figure 9, where $W = 75\,\mathrm{m}$ and $H_1 = 2.6363\,\mathrm{m}$. The truss consists of 141 nodes located on two circles with the common centers and half open angles, $\omega = 5\,\mathrm{deg}$. The nodes of the upper layer are located on the circle with the radius $W/\sin\omega\,(\mathrm{m})$, while those of the lower layer are on the circle with the same origin and the radius $(W/\sin\omega) + 1\,(\mathrm{m})$. The displacement of the node (a) in the y-direction is constrained, while the node (b) is pin-supported,

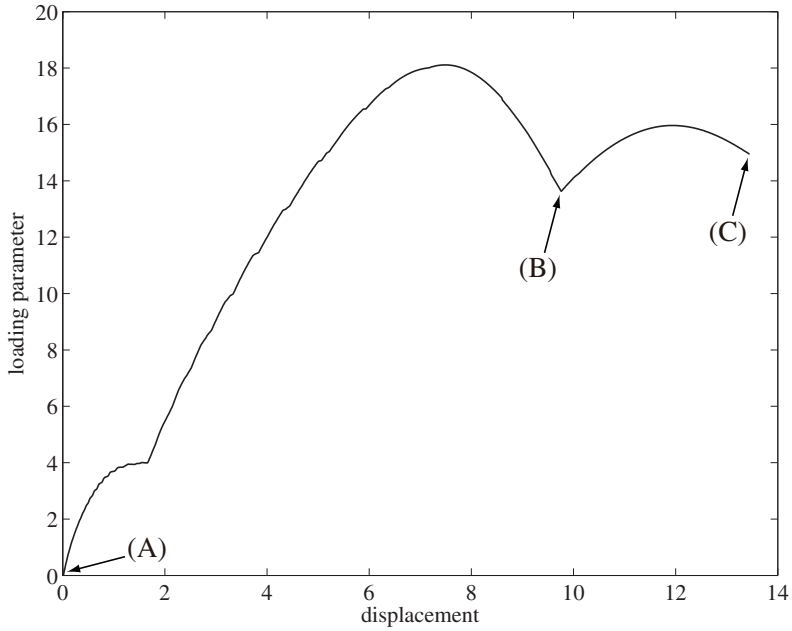

Figure 10: Equilibrium path of the plane truss with curved obstacles.

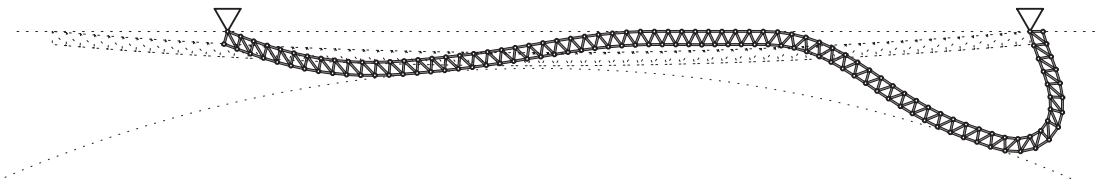

Figure 11: Deformed configuration (solid line) of the plane truss with curved obstacles at the equilibrium state (C) in Figure 10; dotted line: undeformed configuration.

and hence $d = 279$. The truss is located between two fixed rigid obstacles. The upper obstacle has a flat horizontal surface, on which the nodes (a) and (b) are located. The surface of the lower obstacle is defined as a circle with the radius of 100 m, and at the initial configuration there exists a gap of $H_2 = 0.1$ m between the lower obstacle and the center node of the lower layer. Since the nodes of the lower layer may also contact with the upper obstacle, we consider $n_c = 71 \times 2 + 68 = 210$ contact candidates.

The proportional load λ kN is applied at the node (a) in the x-direction. The arc-length constraint is given by $\|(\Delta \boldsymbol{u}, \Delta\lambda)\|_2 = \bar{\theta}$ with $\bar{\theta} = 0.1$. The elastic modulus is 20 GPa. The cross-sectional areas of members in groups (1), (2), (3), (4), ... shown in Figure 6 are given as $0.73\,\mathrm{m}^2$, $0.71\,\mathrm{m}^2$, $0.69\,\mathrm{m}^2$, $0.67\,\mathrm{m}^2, \ldots$, respectively.

The obtained equilibrium path is plotted in Figure 10, which shows the variation (A)→(B)→(C) of the loading parameter λ with respect to the displacement of the node (a). The equilibrium state (B) corresponds to a nonsmooth limit point. Figure 10 depicts the deformed configuration at the equilibrium state (C) in Figure 10.

The number of iterations required at each loading step is listed in Table 2. It is observed that the

Table 2: Number of iterations required at each loading step of the plane truss with curved obstacles.

# of iterations	3	4	5	6	7	8	9	10	12
frequency	1081	379	100	6	7	10	9	10	2

solution is found within four iterations at almost all loading steps, and hence our implicit formulation can enjoy warm start conditions.

6 Conclusions

A non-interior point method has been proposed for frictionless contact problems which can exploit the warm start condition in the arc-length method. We have proposed an implicit formulation of complementarity problems based on the smoothed Fischer–Burmeister function, where the smoothing parameter ρ is considered as an independent variable. By adding a nonlinear equation so that ρ vanishes automatically at the solution of the implicit formulation, we have reduced the governing equations of frictionless contact to a system of nonlinear equations which are continuously differentiable at almost all points. It has been shown that the solution at the previous loading stage in the arc-length method can be used as a good initial point for the current loading stage with a warm start condition. In numerical examples we have demonstrated that in many cases a conventional solver of nonlinear equations converges to the solution within four iterations.

Acknowledgments

This work is supported by a Grant-in-Aid for Scientific Research from the Ministry of Education, Culture, Sports, Science and Technology of Japan.

References

[1] Björkman, G., Path following and critical points for contact problems, *Computational Mechanics*, **10** (1992) 231–246.

[2] Chen, B. and Chen, X., A global and local superlinear continuation-smoothing method for $P_0 + R_0$ and monotone NCP, *SIAM Journal Optimization*, **7** (1997) 403–420.

[3] Crisfield, M.A., A fast incremental/iterative solution procedure that handles "snap-through", *Computers & Structures*, **13** (1981) 55–62.

[4] Christensen, P., A semi-smooth Newton method for elasto-plastic contact problems, *International Journal of Solids and Structures*, **39** (2002) 2323–2341.

[5] Christensen, P., Klarbring, A., Pang, J.-S. and Strömberg, N., Formulation and comparison of algorithms for frictional contact problems, *International Journal for Numerical Methods in Engineering*, **42** (1998) 145–173.

[6] Christensen, P. and Pang, J.-S., Frictional contact algorithms based on semismooth Newton methods, In: Fukushima, M., Qi, L. (Eds.), *Reformulation—Nonsmooth, Piecewise Smooth, Semismooth and Smoothing Methods*, Kluwer Academic Publishers, Dordrecht, 81–116.

[7] De Luca, T., Facchinei, F. and Kanzow C. A semismooth equation approach to the solution of nonlinear complementarity problems, *Mathematical Programming*, **75** (1996) 407–439.

[8] De Luca, T., Facchinei, F. and Kanzow C. A theoretical and numerical comparison of some semismooth algorithms for complementarity problems, *Computational Optimization and Applications*, **16** (2000) 173–205.

[9] Facchinei, F. and Pang, J.-S., *Finite-Dimensional Variational Inequalities and Complementarity Problems*, Springer-Verlag, New York, 2003.

[10] Hu, Z.Q., Soh, A.-K., Chen, W.J., Li, X.W. and Lin, G., Non-smooth nonlinear equations methods for solving 3D elastoplastic frictional contact problems, *Computational Mechanics*, **39** (2007) 849–858.

[11] Jian, J.-B., A superlinearly convergent implicit smooth SQP algorithm for mathematical programs with nonlinear complementarity constraints, *Computational Optimization and Applications*, **31** (2005) 335–361.

[12] Jiang, H. and Ralph, D., Smooth SQP methods for mathematical programs with nonlinear complementarity constraints, *SIAM Journal on Optimization*, **10** (2000) 779–808.

[13] Kanno, Y., An implicit formulation of robust structural optimization under load uncertainties, submitted to *Computers & Structures*.

[14] Kanno, Y., Martins, J.A.C. and Pinto da Costa A., Three-dimensional quasi-static frictional contact by using second-order cone linear complementarity problem, *International Journal for Numerical Methods in Engineering*, **65** (2006) 62–83.

[15] Kanno, Y. and Ohsaki, M., Contact analysis of cable networks by using second-order cone programming, *SIAM Journal on Scientific Computing*, **27** (2006) 2032–2052.

[16] Kanzow, C., Some noninterior continuation methods for linear complementarity problems, *SIAM Journal on Matrix Analysis and Applications*, **17** (1996) 851–868.

[17] Kojima, M., Noma, T. and Yoshise, A., Global convergence in infeasible-interior-point algorithms, *Mathematical Programming*, **65** (1994) 43–72.

[18] Koo, J.S. and Kwak, B.M., Post-buckling analysis of nonfrictional contact problems using linear complementarity formulation, *Computers & Structures*, **57** (1995) 783–794.

[19] Koo, J.S. and Kwak, B.M., Post-buckling analysis with frictional contacts combining complementarity relations and an arc-length method, *International Journal for Numerical Methods in Engineering*, **39** (1996) 1161–1180.

[20] Laursen, T.A., *Computational Contact and Impact Mechanics*: *Fundamentals of Modeling Interfacial Phenomena in Nonlinear Finite Element Analysis*, Springer-Verlag, Berlin, 2002.

[21] Leung, A.Y.T., Chen, G. and Chen, W., Smoothing Newton method for solving two- and three-dimensional frictional contact problems, *International Journal for Numerical Methods in Engineering*, **41** (1998) 1001–1027.

[22] Li, D. and Fukushima, M., Smoothing Newton and quasi-Newton methods for mixed complementarity problems, *Computational Optimization and Applications*, **17** (2000) 203–230.

[23] Miersemann, E. and Mittelmann, H.D., Continuation for parameterized nonlinear variational inequalities, *Journal of Computational and Applied Mathematics*, **26** (1989) 23–34.

[24] Nocedal, J. and Wright, S.J., *Numerical Optimization*, (2nd.ed.), Springer, New York, 2006.

[25] Pang, J.-S., Newton's method for B-differentiable equations, *Mathematics of Operations Research*, **15** (1990) 311–341.

[26] Pieraccini, S., Gasparo, M.G. and Pasquali, A., Global Newton-type methods and semismooth reformulations for NCP, *Applied Numerical Mathematics*, **44** (2003) 367–384.

[27] Pietrzak, G. and Curnier, A., Large deformation frictional contact mechanics: continuum formulation and augmented Lagrangian treatment, *Computer Methods in Applied Mechanics and Engineering*, **177** (1999) 351–381.

[28] Potra, F.A. and Ye, Y., Interior-point methods for nonlinear complementarity problems, *Journal of Optimization Theory and Applications*, **88** (1996) 617–642.

[29] Qi, H.-H. and Liao, L.-Z., A smoothing Newton method for general nonlinear complementarity problems, *Computational Optimization and Applications*, **17** (2000) 231–253.

[30] Qi, L. and Sun, J., A nonsmooth version of Newton's method, *Mathematical Programming*, **58** (1993) 353–367.

[31] Qi, L. and Sun, D., Smoothing functions and smoothing Newton method for complementarity and variational inequality problems, *Journal of Optimization Theory and Applications*, **113** (2002) 121–147.

[32] Sung, J.H. and Kwak, B.M., Large displacement dynamic analysis with frictional contact by linear complementarity formulation, *Computers & Structures*, **80** (2002) 977–988.

[33] Sim, C., csolve, `http://sims.princeton.edu/yftp/optimize/`.

[34] The MathWorks, Inc., *Using MATLAB*, The MathWorks, Inc., Natick, MA, 2008.

[35] Tseng, P., An infeasible path-following method for monotone complementarity problems, *SIAM Journal on Optimization*, **7** (1997) 386–402.

[36] Vanderbei, R.J. and Shanno, D.F., An interior-point algorithm for nonconvex nonlinear programming, *Computational Optimization and Applications*, **13** (1999) 231–252.

[37] Wang, T., Monteiro, R.D.C. and Pang, J.-S., An interior point potential reduction method for constrained equations, *Mathematical Programming*, **74** (1996) 159–195.

[38] Wriggers, P., *Computational Contact Mechanics*, (2nd.ed.), Springer–Verlag, Berlin, 2006.

[39] Xu, S. and Burke, J.V., A polynomial time interior-point path.following algorithm for LCP based on Chen–Harker–Kanzow smoothing techniques, *Mathematical Programming*, **86** (1999) 91–103.

[40] Zavarise, G., Wriggers, P. and Schrefler, B.A., A method for solving contact problems, *International Journal for Numerical Methods in Engineering*, **42** (1998) 473–498.

[41] Zhang, H.W., He, S.Y. and Li, X.S, Non-interior smoothing algorithm for frictional contact problems, *Applied Mathematics and Mechanics*, **25** (2004) 47–58.

[42] Zhang, H.W., He, S.Y., Li, X.S. and Wriggers, P., A new algorithm for numerical solution of 3D elastoplastic contact problems with orthotropic friction law, *Computational Mechanics*, **34** (2004) 1–14.

[43] Zhang, X., Jiang H. and Wang, Y., A smoothing Newton-type method for generalized nonlinear complementarity problem, *Journal of Computational and Applied Mathematics*, **212** (2008) 75–85.

[44] Zhao, Y.B. and Li, D., A new path-following algorithm for nonlinear P_* complementarity problems, *Computational Optimization and Applications*, **34** (2005) 183–214.